On multiple states in single-layer flows

Peter G. Baines

CSIRO Atmospheric Research, Aspendale 3195, Australia

J. A. Whitehead

Woods Hole Oceanographic Institution, Woods Hole, Massachusetts 02543

For free surface flows over obstacles in a channel of constant width, there is a range of parameter values where two steady flow states are possible, with the state that is actually obtained being determined by the past history. Specifically, one of these flow states is wholly supercritical (i.e., no waves can propagate upstream against the flow) over the obstacle. The other has a hydraulic jump that travels to upstream infinity, and the flow undergoes a subcritical (i.e., waves can propagate in both directions) to supercritical transition at the obstacle crest. A new, third steady solution is described here, in which a hydraulic jump is stationary over the upstream face of a long obstacle. This new solution is contiguous with the other two, and in a sense, lies between them. It is shown that this new solution is unstable, in that if the stationary jump is displaced to a location with a slightly different bottom height, it will move further in the same direction. By this criterion, jumps are unstable on upslope flow, and stable on downslope flow. These properties, and the general character of hysteresis implied by these multiple hydraulic equilibria, have been tested with two series of experiments. The new solution is ordinarily not found because of its instability, but it can be viewed by manually balancing the unstable jump. Comparisons were also made between the observed abrupt transitions between flow states, and the predictions of hydraulic theory. Qualitatively the agreement is quite good, with differences attributable to experimental factors that are not contained in two-dimensional long wave hydraulics. © *2003 American Institute of Physics.* [DOI: 10.1063/1.1531178]

I. INTRODUCTION

Hydraulic solutions for flow of a single layer over a long obstacle of maximum elevation h_m are known to possess two possible steady solutions within a certain range of flow parameters. If the flow is commenced at some initial time with an initial fluid speed U, initial fluid depth d_0, the resulting steady flow states are determined by the initial Froude number $F_0 = U/(g d_0)^{1/2}$ and the height ratio $H_m = h_m/d_0$, and there are five main flow types as shown in Fig. 1.[1] In the region GAE, two different locally steady flow states are possible, and the solution obtained in practice depends on the manner in which the flow is established, as shown, for example, by Pratt.[2] In one of these solutions the flow is supercritical everywhere—the local Froude number $F > 1$ everywhere, and linear waves (i.e., small disturbances) cannot progress upstream against the flow. In the other, the flow undergoes a transition from subcritical to supercritical at the crest of the obstacle, and a hydraulic jump progresses to upstream infinity, effectively altering the flow state upstream of the obstacle. This "multiple state" regime has been known for at least the past 20 years.[3]

An alternative description of these flow states has been given by Lawrence,[4] who chooses as the basic variables d_c/h_m and d_0/h_m (in present notation), where d_c denotes the layer thickness at the obstacle crest. These variables provide a less comprehensive picture, but they are convenient for discussing locally steady flows where the total flow rate is specified and flow at the obstacle crest is critical, and a regime diagram corresponding to Fig. 1 results. Lawrence also verified the multiple-state/hysteresis phenomenon experimentally, and showed that when upstream jumps were produced, friction could cause them to become stationary at finite distances upstream of the obstacle.

One may ask whether a hybrid of these two "multiple states" is possible, in which the upstream flow is supercritical, but a stationary hydraulic jump exists over the upstream face of the obstacle. This would give a supercritical to subcritical transition over the upstream face, with a subcritical to supercritical transition further downstream at the obstacle crest. Such solutions do in fact exist, as demonstrated in the next section, and the new solutions provide a continuous junction between the other two. However, these new solutions are unstable, as shown in Sec. III. This has been investigated experimentally as described in Sec. IV. Flow states that correspond to the previously known stable states are found. There is a considerable range of observed hysteresis, although this is smaller than predicted. A laboratory device has been constructed which enables an operator to balance the unstable solution and thus allow it to persist indefinitely. This situation is of interest because it is perhaps the simplest example in fluid mechanics of hysteretic three-state flow, it may be readily demonstrated experimentally, and it gives intuition concerning more complex flows containing similar properties.
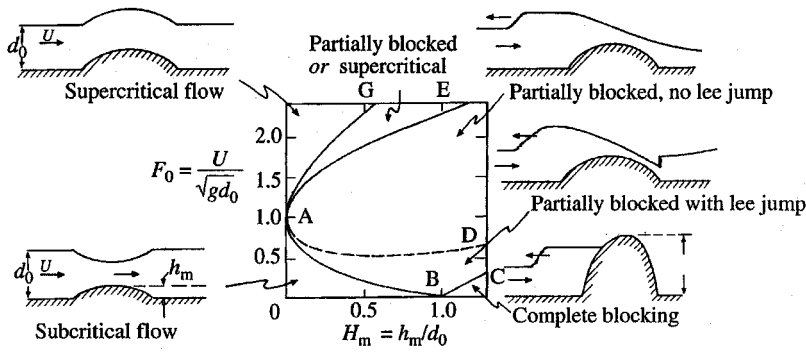
FIG. 1. Flow regimes on the F_0-H_m diagram for hydrostatic single-layer flow over an obstacle.

II. A NEW SOLUTION TO THE FLOW UPSTREAM OF AN OBSTACLE

We consider the flow of a layer of fluid of thickness $d(x,t)$ and velocity $u(x,t)$ in a channel of uniform width, over a long obstacle of height $h(x)$. The essential equations and assumptions are standard and are given in Baines[1] (Sec. 2.3). We write $d=d_0+\eta-h$, where d_0 is an equilibrium depth and η is the interface displacement; u and d are then governed by

$$u_t+uu_x=-g\,\eta_x, \tag{1}$$

$$d_t+(du)_x=0. \tag{2}$$

A hydraulic jump is represented by an abrupt increase in depth of the fluid layer, and if the upstream and downstream values of d and u are given by d_u, u_u, and d_d and u_d, respectively, the speed of the jump c_J relative to the upstream fluid is given by

$$c_J^2=\frac{gd_d}{2}\left(1+\frac{d_d}{d_u}\right). \tag{3}$$

The flow is characterized by the Froude number F, defined by $F^2=u^2/gd$.

We consider flow that is uniform and supercritical upstream of the obstacle, and look for steady solutions of Eqs. (1), (2) in which there is a stationary hydraulic jump situated over the upstream face of the obstacle, as shown schematically in Fig. 2. If U and d_0 are the upstream values of u and d, the upstream Froude number is given by

$$F_0=\frac{U}{(gd_0)^{1/2}}, \tag{4}$$

which has values greater than 1 for supercritical flow. With notation as indicated in Fig. 2, the steady-state forms of Eqs. (1), (2) show that the flow state is specified by

$$Q\equiv Ud_0=u_cd_c=u_ud_u=u_dd_d, \tag{5}$$

$$u_c^2=gd_c, \tag{6}$$

$$\frac{1}{2}U^2+gd_0=\frac{1}{2}\frac{Q^2}{d_u^2}+g(d_u+h_j), \tag{7}$$

$$\tfrac{1}{2}u_d^2+g(d_d+h_j)=\tfrac{1}{2}u_c^2+g(d_c+h_m), \tag{8}$$

$$u_u^2=\frac{gd_d}{2}\left(1+\frac{d_d}{d_u}\right), \tag{9}$$

where h_m is the maximum topographic height (this obstacle is termed a "weir" in the present experiments). Here Eq. (5) is given by the conservation of mass flux, Eq. (6) by the critical condition at the obstacle crest, Eqs. (7) and (8) by the Bernoulli equation each side of the jump, and Eq. (9) from the conditions across the jump in the form (3). These seven equations contain seven unknowns: h_j, u_u, d_u, u_d, d_d, u_c, and d_c. To nondimensionalize, we define

$$D=\frac{d}{d_0}, \quad D_u=\frac{d_u}{d_0}, \quad D_d=\frac{d_d}{d_0}, \quad H=\frac{h}{d_0}, \quad H_m=\frac{h_m}{d_0}. \tag{10}$$

Examination of the above equations shows that they only have physically relevant solutions inside the region GAE of Fig. 1. This is the region of H_m-F_0 space in which flow over long obstacles [governed by Eqs. (1), (2)] has two solutions, as described above.

In order to compute the location (specified by the bottom elevation) and amplitude of the stationary jump from Eqs. (5)–(9), we first fix F_0 and the (scaled) depth on the upstream side of the jump, D_u, which must lie in the range $1<D_u<F_0^{2/3}$. The topographic height at this point is then given by Eq. (7) in the form

$$H_j=\frac{h_j}{d_0}=(1-D_u)\left[1-\frac{F_0^2}{2}\frac{(1+D_u)}{D_u^2}\right], \tag{11}$$

where $0<H_j<H_m$. The depth downstream of the stationary jump is then given by Eq. (9), which gives
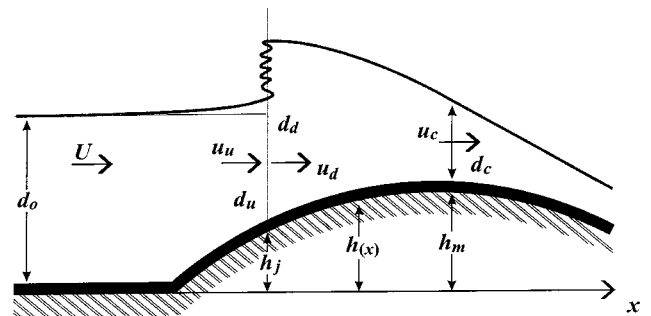

FIG. 2. Schematic diagram showing a stationary hydraulic jump (relative to the ground) over the upstream face of an obstacle, with notation.

$$D_d = \frac{1}{2}\left[D_u^2 + 8\frac{F_0^2}{D_u}\right]^{1/2} - \frac{D_u}{2}, \tag{12}$$

so that the jump amplitude is given by $D_d - D_u$. The maximum topographic height H_m is then given by Eqs. (5), (6), and (8), which is

$$H_m = 1 + \frac{F_0^2}{2} - \frac{3}{2}F_0^{2/3} - (D_d - D_u)\left[\frac{F_0^2}{2}\frac{(D_d + D_u)}{D_u^2 D_d^2} - 1\right]. \tag{13}$$

Exploring these conditions in parameter space (H_m, F_0) shows that solutions exist within the region GAE of Fig. 1, but not outside it. Hence there are three stationary solutions for hydrostatic flow over an obstacle inside GAE, but only one outside (i.e., all three solutions are equal outside GAE). We describe these new solutions in terms of the jump height D_j, defined as $D_j = D_d - D_u$. Figures 3(a) and 3(b) show the known stable solutions. Figure 3(a) shows the solution in BAE with the upstream jump extending to AG (termed solution I), and Fig. 3(b) shows the supercritical solution above AG extending down to AE (termed solution II). The corresponding jump amplitudes for the new solution (solution III) are shown in Fig. 3(c). One sees that it is contiguous with both of the others, equalling the solution in Fig. 3(b) at AG, and that of Fig. 3(a) at AE, where the jump height rapidly becomes zero as AE is approached from AG. Along AG, solutions I and III are equal, with an effectively stationary jump at the upstream end of the obstacle (where $h = 0$). As F_0 decreases toward AE, the speed of the upstream jump in solution I increases, and it propagates away upstream, whereas in solution III the jump remains stationary and retreats downstream up the face of the obstacle, with decreasing amplitude. As curve AE is approached, the jump amplitude in solution III decreases rapidly to zero and the solution approaches the wholly supercritical state. On crossing AE, solution III changes abruptly to solution I, as does solution II.

III. THE STABILITY OF UPSTREAM HYDRAULIC JUMPS OVER TOPOGRAPHY

We consider the stability of a steady solution of a stationary hydraulic jump situated over sloping topography, in a similar manner to that described in Sec. II. Since we are only considering small perturbations, we may assume that the topography consists of a plane slope. The steady solution is given by

$$u_u d_u = u_d d_d = Q, \tag{14}$$

implying mass flux conservation as in Eq. (5), and momentum flux conservation

$$d_u u_u^2 + \tfrac{1}{2}g d_u^2 = d_d u_d^2 + \tfrac{1}{2}g d_d^2, \tag{15}$$

which implies Eq. (9). We next consider a small perturbation to this steady state, in which the perturbed jump has (small) speed c, and departures from the steady values are denoted by primes. Taking axes moving with the jump at speed "c," corresponding to Eqs. (14), (15) we have

$$(u_u + u_u' - c)(d_u + d_u') = (u_d + u_d' - c)(d_d + d_d'), \tag{16}$$

$$(d_u + d_u')(u_u + u_u' - c)^2 + \tfrac{1}{2}g(d_u + d_u')^2$$
$$= (d_d + d_d')(u_d + u_d' - c)^2 + \tfrac{1}{2}g(d_d + d_d')^2. \tag{17}$$

We ask whether the jump in the new region adopts a velocity which moves it back to the original location, or away from that location. Mathematically the objective is to calculate c. For a very small change in bottom depth, it can be assumed that the primed quantities are small compared to their unprimed counterparts.

The flow is supercritical on the upstream side of the jump, whether moving or stationary, and subcritical on the downstream side. It follows that for a perturbed and possibly moving jump, the flow on the upstream side will be undisturbed, but that the flow on the downstream side may be. However, the moving jump is now at a slightly different location, and consequently different depth and mean flow. Hence

$$(u_u + u_u')(d_u + d_u') = Q, \tag{18}$$

so that after linearizing, we have

$$u_u' d_u + d_u' u_u = 0, \tag{19}$$

and with Eq. (16)

$$c(d_d - d_u) = u_d d_d' + d_d u_d'. \tag{20}$$

The Bernoulli function on the upstream side (relative to fixed axes) will be unchanged, so that

$$\tfrac{1}{2}u_u^2 + g d_u = \tfrac{1}{2}(u_u + u_u')^2 + g(d_u + d_u' - \delta), \tag{21}$$

where the change in topographic height is $-\delta$. This gives

$$d_u' = \delta - \frac{u_u}{g}u_u'. \tag{22}$$

Equations (19) and (22) give

$$d_u' = \frac{\delta}{1 - F_u^2}, \quad u_u' = -\frac{u_u}{d_u}\frac{\delta}{1 - F_u^2}, \quad F_u^2 = \frac{u_u^2}{g d_u}, \tag{23}$$

and Eqs. (16) and (17) then give

$$c = u_u' - \frac{g d_d}{4 u_u}\left[\left(1 + \frac{2 d_d}{d_u}\right)\frac{d_d'}{d_d} - \frac{d_d}{d_u}\frac{d_u'}{d_u}\right]. \tag{24}$$

In order to obtain an equation for c in terms of $-\delta$, we need an extra condition on d_d' and u_d', which will depend on the circumstances further downstream. There are two distinct possibilities: (i) assume that there is no effect from further downstream that influences the jump, and (ii) assume a downstream control (or other condition) that fixes the value of the Bernoulli function downstream of the jump. We discuss these in turn.

A. Case (i)

In general, perturbations to the jump will cause perturbations to the flow immediately downstream of it. Assuming that these changes are not influenced by any factors further downstream, or equivalently, that there is no downstream source of waves propagating in the upstream direction to-
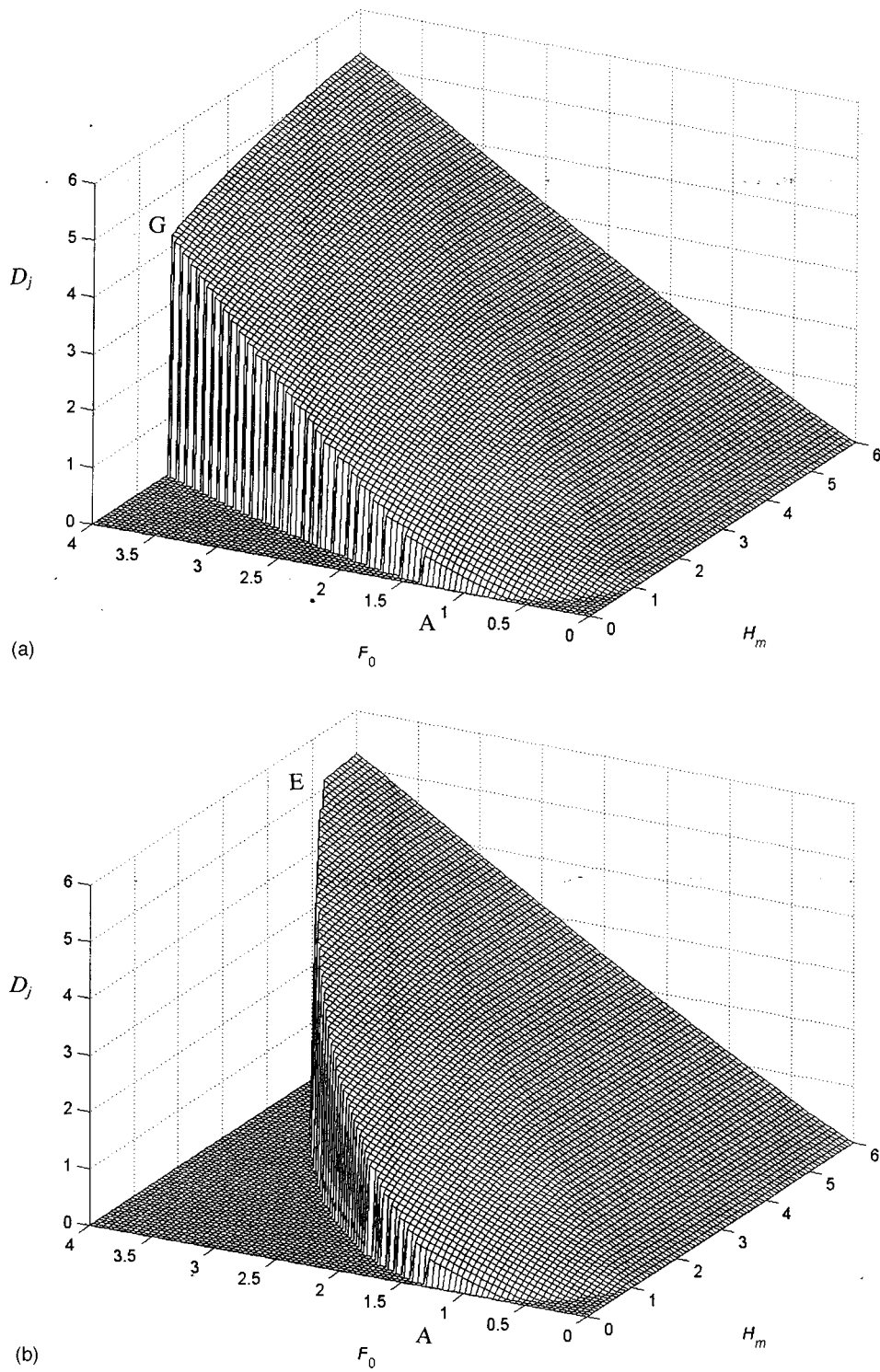
FIG. 3. (a) The theoretical upstream jump height $D_j = D_d - D_u$ as a function of F_0 and H_m for the solution with upstream disturbances in the region GAE. (b) The same as (a), but for the solution that is wholly supercritical in region GAE. (c) The upstream jump height D_j for the new third solution, where the jump is stationary over the upstream face of the topography, as depicted in Fig. 2. The jump height decreases rapidly to zero as the curve AE is approached, and the jump approaches the obstacle crest.

ward the jump, the equation for the appropriate "Riemann invariant" applies. This may be expressed in the form Baines[1] [Eqs. (2.3.4), (2.3.5)]

$$\frac{d}{dx}(u - 2(gd)^{1/2}) = -\frac{g}{u - (gd)^{1/2}}\frac{dh}{dx}, \tag{25}$$

which for small changes gives

$$d(u - 2(gd)^{1/2}) = -\frac{g}{u - (gd)^{1/2}}dh. \tag{26}$$

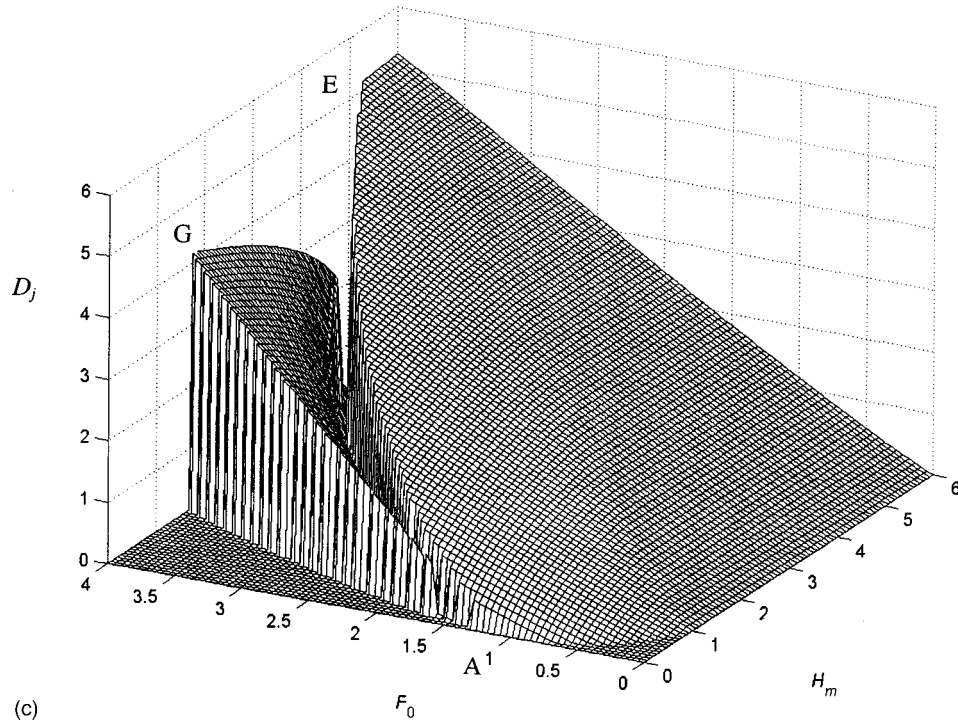Applying this to conditions immediately downstream of the jump, with $dh = -\delta$, we have

(c)

FIG. 3. (*Continued.*)

.

$$u'_d = \left(\frac{g}{d_d}\right)^{1/2}\left(d'_d - \frac{\delta}{1-F_d}\right), \quad F_d^2 = \frac{u_d^2}{g d_d}, \tag{27}$$

and substituting this into Eq. (20) gives

$$d'_d = \frac{c}{(g d_d)^{1/2}} \frac{(d_d - d_u)}{(1+F_d)} + \frac{\delta}{1-F_d^2}. \tag{28}$$

Substituting Eqs. (23) and (28) into Eq. (24) then gives

$$c = -\frac{F_d}{1+F_d} \frac{g d_d}{Q} \delta. \tag{29}$$

This implies a negative change in jump speed for a decrease in bottom height (positive δ), and hence an unstable jump on an upward slope.

B. Case (ii)

If there is a flow feature that lies downstream from the jump that has influence on (or control of) the flow so that it sends disturbances upstream toward the jump and affects it, it may be more realistic to incorporate this into the stability analysis. This applies in the specific case of interest here, namely control at an obstacle crest, which fixes the Bernoulli constant R. Since the flow is subcritical between this control section and the jump, in applying this to the flow we make the assumption that the two are close together, so that disturbances may communicate rapidly between them, maintaining a quasistatic state in this region with no material stored in between.

Corresponding to Eq. (22) we then have

$$u'_d = -\frac{u_u}{d_u} \frac{\delta}{1-F_u^2}, \tag{30}$$

and then from Eq. (20)

$$d'_d = \frac{\delta - c \frac{F_d^2}{u_d}(d_d - d_u)}{1-F_d^2}. \tag{31}$$

Substituting Eqs. (23) and (31) into Eq. (24) then gives

$$c = -\frac{g d_d}{Q} \delta. \tag{32}$$

Hence, both Eqs. (29) and (32) show that perturbed jumps on upward sloping topography move further away from their initial stationary point, implying that these flows are unstable. For downward sloping topography the converse applies, and the jumps are stable.

IV. EXPERIMENTS

There is a lack of experimental studies of hydraulic flows where multiple flow states are predicted by theory. In particular, except for Lawrence's study,[4] the region GAE of Fig. 1 has not been investigated at all in any formal sense. The following experiments were carried out as a step to rectify this, and also to investigate the theoretical flow properties described in the previous sections. In particular, we wondered under what circumstances can one readily produce stationary hydraulic jumps over sloping topography? Two devices have been constructed that show the hysteresis that is

predicted from the above. The first is a flume (which is a channel that supports a continuous flow from one end to the other) that was made so that it could contain an hydraulic jump upstream of an obstacle. The second device, or flume, enabled the observation of upslope flow with the obstacle curvature zero in order to come closer to the long wave approximation.

Analysis of the preceding sections is inviscid, but in order to accommodate experimental convenience and reality, it is necessary to include two additional factors. The first of these is frictional drag, effected by means of a drag coefficient, and the second is a tilted channel floor, as a convenient means of driving the flow. Both of the sets of experiments have been carried out in a flume, tilted at angle θ to the horizontal, with the convention that $\theta > 0$ for downward slope in the direction of flow. With the added frictional drag term, Eq. (1) becomes

$$u_t + u u_x + g \eta_x = -C_D u^2/d, \tag{33}$$

where $\eta = d + h(x)$, x is horizontal, η and d are measured vertically, and C_D is the frictional drag coefficient. The principal parameter for these flows is again the local Froude number, F. The parameter to be varied in the experiments is the tilt angle θ, which results in changes to the Froude number. For steady flows where $du = Q$, $F^2 = (d_s/d)^3$, where $d_s = (Q^2/g)^{1/3}$. In downslope flows, a steady state in which u and d are constant with x is possible, where the downslope buoyancy term $g \sin \theta$ balances the drag; with this as the mean state, hysteresis phenomena do not arise (Baines,[1] Sec. 2.3.4). However, in these experiments this balance is not realized because the viscous drag is too small and (equivalently) the flume is too short. For these experiments θ is in the range $5° < \theta < 8°$ and C_D has values[5] of order 0.004 (for Reynolds numbers of order 10^4), implying that frictional drag is small but not entirely negligible. Fluid effects generated by flow over an obstacle should therefore be locally small. Friction may have secular effects on waves propagating away from the obstacle, and hence be substantial at large distances from it (Lawrence[4]), but they should remain small in the short tanks used here. For steady flow over featureless sloping terrain, Eqs. (33), (2) give

$$\frac{dd}{dx} = -\frac{dh/dx - C_D F^2}{F^2 - 1}. \tag{34}$$

Hydraulic jumps [governed by Eq. (3)] may be inserted into such flows. Stationary jumps may exist on flows down slopes, since the decrease in fluid depth behind the jump as it propagates upslope decreases the jump speed, to the point where it vanishes [from Eq. (8)].

With these theoretical preliminaries, we begin with a description of the experiments with the first flume. As sketched in Fig. 4, this experiment was done in a uniform channel, 1 m long, 0.07 m deep, and of width $w = 0.05$ m. An obstacle was placed in it with the shape of a smooth weir that was elevated 0.038 m above the horizontal floor of the channel. The obstacle crest was 0.3 m from the downstream end of the tank. Near the upstream end a sluice was constructed using a
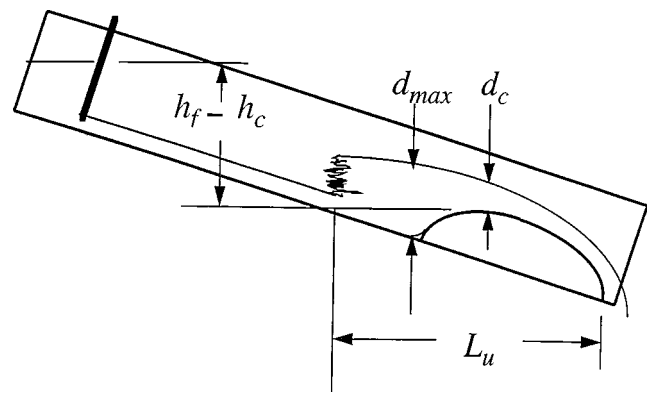

FIG. 4. The tank design and the measured flow parameters of the first set of experiments. The sluice gate is denoted by the thick line on the left, and the flow is from left to right.

small sliding gate held in grooves in the sidewall. The channel was held at an adjustable angle so that the elevation of the floor of the sluice was above the crest of the obstacle. This ensured that supercritical flow could arrive at the crest of the obstacle, given sufficient tilt of the channel bottom and small friction. The lower, downstream end of the flume extended over a large basin filled with water so that water flowing downstream of the crest could spill into the basin. Water was pumped from this basin into a small region upstream of the sluice gate at a fixed, controlled volumetric flow rate Q_v. This rate was carefully controlled at a constant flux for each set of observations and monitored with a flow meter with accuracy of approximately 5%. The gap at the bottom of the sluice was set at a size sufficient to allow water to accumulate to a level of about 0.05 m above the gap, and enter the channel as a supercritical flow. This current would then flow down along the tilted bottom of the channel, where it would encounter the obstacle. The size of the apparatus and the flow rates were selected for ease of handling, and to minimize frictional loss of the flow; smaller apparatuses would be subject to molecular viscosity.

Water speed downstream of the sluice gate was governed by two factors: first, the height of the sluice gate opening, which was kept fixed, and second, by the angle of the channel. This was set using a labjack that was placed under the upstream end of the channel. A side-view of the water was recorded using a video camera. The water was dyed to enable the surface to be seen clearly. Thirty-five-mm slide photographs of selected runs were also taken, using a uniformly lit white background. In these experiments the upstream fluid emerging from the sluice was always supercritical. This flow remained supercritical as it moved down the channel (until it encountered an obstacle or hydraulic jump), but the thickness and speed varied according to Eq. (33) because of the sloping channel.

The experimental procedure was as follows. The flume angle θ was set at a small value, and the sluice gate was opened. Observations were then made after the flow had adjusted to steady-state, with a form as shown in Fig. 4: supercritical flow upstream, with a stationary upstream hydraulic jump to subcritical flow, and then critical flow at the obstacle crest. Measurements were taken by hand with rulers, but
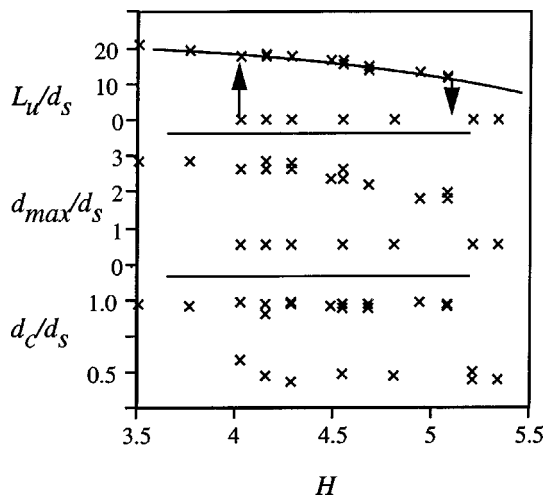
FIG. 5. Some measured features that display hysteresis as the elevation of the upstream reservoir, $H=(h_f-h_c)/d_s$, is varied in the first experiment. The top panel displays the (scaled) upstream position (distance from the rear of the obstacle) of the hydraulic jump. The middle panel shows the maximum water thickness; this is located upstream of the crest in the place where the bottom is deepest. The bottom shows the water thickness at the crest of the weir. For these experiments $Q_\nu=340$ cm^3 s^{-1}.
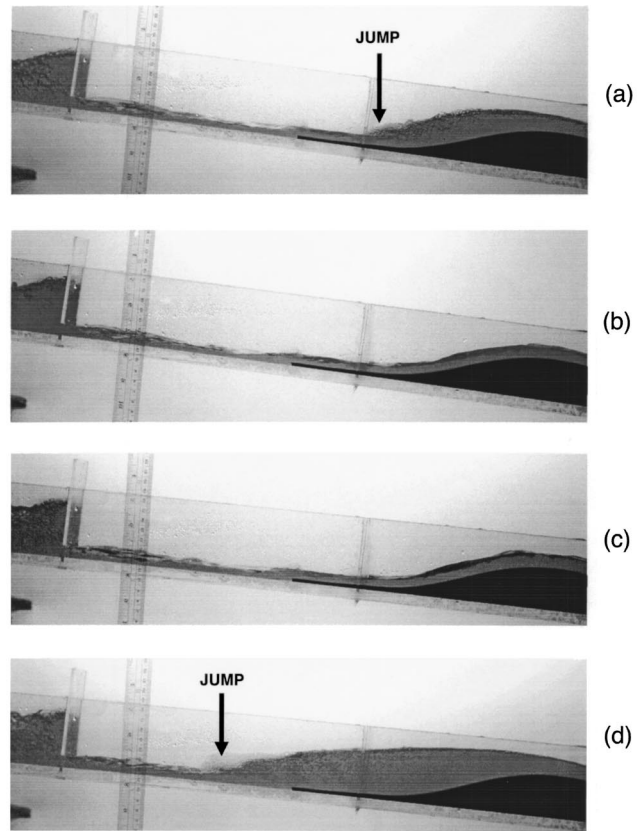

FIG. 6. Flow in a channel for tilt angles near transition values of the hysteresis range. Flow is from left to right, and all flows are approximately steady. The crest of the weir is the highest part of the crescent shaped black region on the far right. To the left is the sluice gate. (a) Subcritical flow $H=5.05$, (b) supercritical flow $H=5.10$, (c) supercritical flow $H=4.04$, and (d) subcritical flow $H=4.03$.

were found to be inferior to on-screen measurements from videotape, which was recorded for all runs. This method was found to be sufficiently precise for these data, as the presence of near-random surface waves limited the resolution that was possible. The labjack setting was then increased by about 2 or 3 mm, and a new run was carried out, repeating the measurement process. At each setting, the video images and the slides were taken after noting that the flow achieved steady state. This procedure was repeated until the flow was observed to be wholly supercritical, after which the angle θ was increased once more. The experiment was then continued with θ being decreased in corresponding steps with the same observational procedure at each step, until finally the upstream jump and subcritical flow were again observed. The whole procedure was then repeated a number of times, and then repeated again for a different flow rate.

From the video images, measurements were taken of the following four dimensions, which are also shown in Fig. 4: (1) distance of the location of the hydraulic jump upstream to the right-hand edge of the obstacle, L_u; (2) maximum thickness of water upstream of the crest, $d_{\max}$; (3) thickness of water at the crest of the weir, d_c; and (4) elevation of the free water surface in the reservoir h_f minus elevation of the crest of the weir, h_c. As h_f-h_c was systematically varied up and down, a "hysteresis loop" was found for both flow rates. The results for the fastest flow rate ($Q_\nu=340$ cm^3 s^{-1}) are shown in Fig. 5. This contains measurements of L_u, $d_{\max}$, and d_c. These are divided by the depth scale $d_s=(Q_\nu^2/w^2g)^{1/3}=(Q^2/g)^{1/3}$, which is the theoretical thickness of a critically controlled flow of two-dimensional flow rate Q at the crest of a critically controlling weir. They are plotted against $H=(h_f-h_c)/d_s$, which is the scaled elevation difference between the free water surface level in the reservoir, h_f, and the scaled elevation of the crest of the weir, h_c. The data show two values of each dependent variable for the

same value of H over the interval $3.75<H<5.25(\pm0.10)$. The upper values are interpreted as representing subcritical flow upstream of the obstacle crest, and the lower values represent supercritical flow throughout this region. Results for a slower flow rate were very similar qualitatively but the details differed as one would expect. The transition in the flow state at the larger value of H was seen just as the jump approached the obstacle base. Thus no jump was ever located on the part of the obstacle sloping upward in the direction of the flow. The measurement errors are estimated to be the size of the symbols. The length measurements have relatively large errors due to the difficulty in defining the exact location of the jump in an image.

In Fig. 6, photographs from slides show the multiple equilibrium character of the flow for four different channel tilt angles. Angle values, or the equivalent values of H, are precise to $\pm0.01°$. This is about a factor of 10 smaller than those possible with videotape images used for Fig. 5. The top panel, Fig. 6(a), shows a stationary hydraulic jump just upstream of the obstacle, followed by subcritical flow, with the floor of the channel tilted at an angle of $7.82°$ ($H=5.05$). This angle is close to the upper transition angle (see Fig. 5), and the supercritical flow upstream of the hydraulic jump has pushed the jump almost to the location of the upstream nose of the obstacle. The hydraulic jumps in these experiments are

Phys. Fluids, Vol. 15, No. 2, February 2003

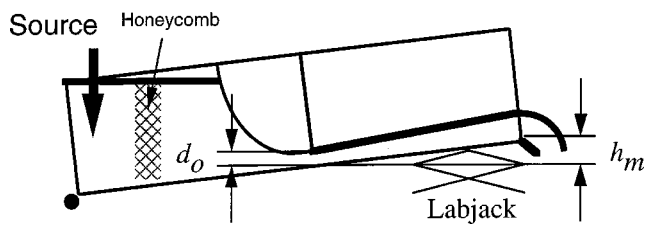On multiple states in single-layer flows   305

FIG. 7. The tank design and measured flow parameters of the second set of experiments.

turbulent, and spread out over a length of 3–4 cm. Hence their positions are not precisely defined, and are complicated by across channel variations (smaller scale experiments with axisymmetric geometry[6–8] give a good picture of along-jump variability). The second panel [Fig. 6(b)] shows supercritical flow at the slightly greater angle of 7.90° ($H = 5.10$). Shortly after the increase in channel slope, we saw the supercritical flow sweep the hydraulic jump downstream over the crest of the obstacle. The third panel [Fig. 6(c)] shows flow in which the angle has been decreased all the way down to 5.95° ($H = 4.04$). For this value the flow is still supercritical, but the angle is just slightly above the angle for transition back to subcritical flow. We saw that trapped waves became prevalent near the crest as the transition value was approached. For example, this panel shows a marginally stable wave at the crest as an irregularity of the surface. The wave was visibly created by a small irregularity at the sidewall along the middle of the channel, but the flow remained steady for minutes in this state. Finally, as soon as the angle was brought down to a very slightly smaller angle of 5.93° ($H = 4.03$) (a change in labjack elevation of only about 1 mm), a wave propagated upstream starting from the crest. It brought the system to the subcritical state shown in the bottom panel of Fig. 5. Here, the upstream depression of the floor was filled with subcritical flow and a stationary hydraulic jump was located further upstream.

Detailed predictions from the hydraulic model, Eqs. (33), (2), may be used to predict the flow properties for comparison with experiment. This has not been done here because the details are complex if frictional drag is included, and the comparison is not meaningful given the limited nature of the observations and the nonhydrostatic character of many of the details. Nevertheless, the fact that the maximum value of d_c / d_s in Fig. 5 is close to unity (within about 15%) indicates that the scaling used in this experiment is appropriate, and that friction is negligible in the vicinity of the crest of the obstacle.

Experiments with the second flume design gave more quantitative data of the multiple state regime, in a form that could be related directly to Fig. 1. In the preceding design, upward centrifugal force from curvature of the weir was sometimes a sizeable percentage of the downward force of gravity. This introduced a large unwanted modification to quantitative calculations. In the second design, the bottom was completely straight so that centrifugal effects were eliminated. In addition, the main operating region was the plane upsloping portion of the flume, to minimize frictional energy loss. The apparatus is sketched in Fig. 7. A channel

1.2 m long, 0.2 m deep, and of width $w = 0.052$ m was used, inclined at a variable angle θ to the horizontal. This channel had a flat glass bottom, and contained a rounded sluice gate made of foam covered with smooth plastic tape in the middle of the passage. The tank was aligned with θ negative (sloping upward in the direction of flow), and water was pumped into the cavity behind the sluice at the lower end. Turbulence here was damped with a honeycomb of loose plastic foam. The water level in this upstream reservoir would build up above the depth of the sluice gate opening, and the pressure produced flow into the downstream, working part of the tank (length 0.6 m), up the tilted channel. The downstream end wall was absent so that water could spill out freely there. As in the previous design, the downstream end of the flume extended over a large catch basin filled with water. Water was pumped from this catch basin into the small upstream reservoir at a fixed volumetric rate Q_v. This rate was carefully controlled and measured to be a constant flux to better than 1% accuracy.

Runs were conducted after setting a sluice gap height of 0.0052, 0.0107, or 0.0153 m. To start, the tilt of the tank was made minimal so that supercritical flow extended downstream of the gate to the end of the flume. Then the tilt was increased by increment so that the elevation of the downstream end progressively became larger than the bottom of the gap. Time for readjustment of the upstream free surface height was allowed to pass after each change in tilt angle. Finally, at a critical elevation of the downstream end, a bore formed over the water surface next to the downstream end, and propagated upstream as an hydraulic jump. This transition is shown in photographs in Fig. 8, panels (a) and (b), and it may be shown from Eqs. (33)–(34) that it corresponds to the curve EA in Fig. 1. The resulting subcritical flow is shown in panel 8(c); the initial increase in layer thickness is part of the initial stationary hydraulic jump, and the subsequent decrease in thickness is in accord with Eq. (34). The tilt was then decreased by increments. At a second critical elevation of the downstream end, the hydraulic jump located at the sluice gate moved downstream to the end of the tank and vanished. This transition is shown in panels (d) through (e) in Fig. 8, and it corresponds to curve AG in Fig. 1.

This experiment permits quantitative comparison between experiment and theory. Using the value of the gap of the sluice gate d_0, the elevation of the floor of the downstream end of the tank over the elevation of the sluice gate, h_m, and the (two-dimensional) volume flux of water $Q = Q_v / w$, we can calculate the values of F_0 and H_m. Their values for the two sets of transitions are shown compared with the inviscid curves AG, AE, and BC in Fig. 9. The qualitative agreement is excellent. A wide gap between the two transitions is found, and both occur within the hysteresis band. Quantitative agreement between experiment and theory differs by tens of percent, and the width of the hysteresis regions in the experiments is less than theory predicts. This is not surprising since the experiments possess a number of additional physical processes (notably shorter and steeper waves, side and bottom boundary layers, waves along the sidewall, a crest that is not level, and some turbu-
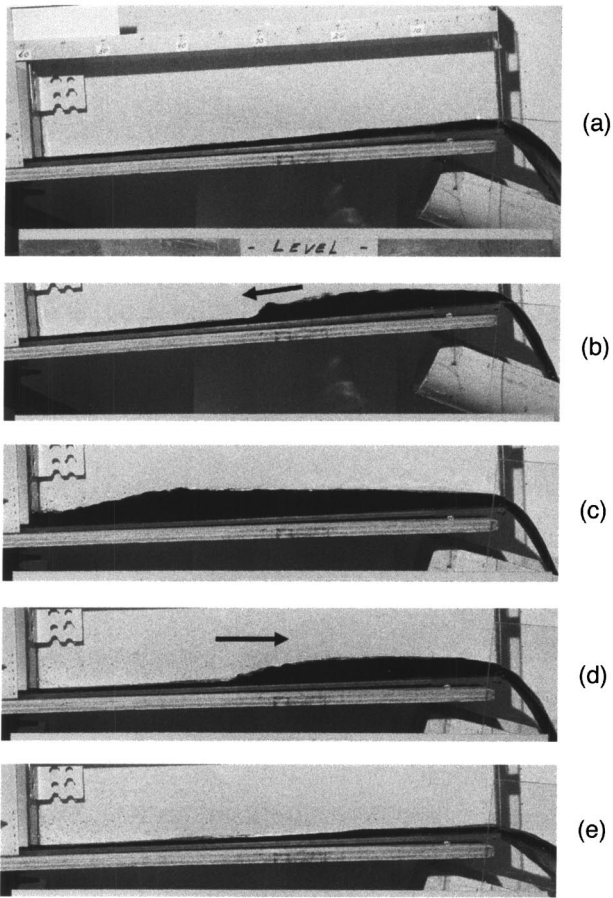
FIG. 8. Photographs of the transitions seen with the second set of experiments. The fluid flows in from the left through a sluice gate and ascends a constant sloping bottom. For this run, $F_0 = 5.6$. (a) Supercritical flow, $H_m = 7.9$. (b) An hydraulic jump moving upstream, triggering a transition to subcritical flow upstream of the crest, $H_m = 8.0$. (c) Subcritical flow in the entire upstream region, $H_m = 6.0$. (d) An hydraulic jump that is moving downstream (up the slope) triggering a transition to supercritical flow, $H_m = 4.4$. (e) A few seconds later with the same parameters.

lence within the flowing water) compared to the theory. It can be shown from Eqs. (33)–(34) that the inclusion of bottom friction alone causes the lower transition curve to rise above AE, consistent with observations. However, the behavior of the upper transition (near AG) depends on the effect of friction on the speed of hydraulic jumps, a more complex process. An additional feature not found in the theory is the presence of stationary solitary wavelike features, which sit upstream of the exit when the flow is slightly supercritical (i.e., to the left of AE).

V. DISCUSSION AND CONCLUSIONS

We have shown that there is an additional solution to flow of a single layer over a long obstacle, in the ranges of values of F_0 and H_m in which two stable solutions are already known to occur (region GAE of Fig. 1). This new solution provides a continuous junction between the other two solutions, but is predicted to be unstable in the sense that
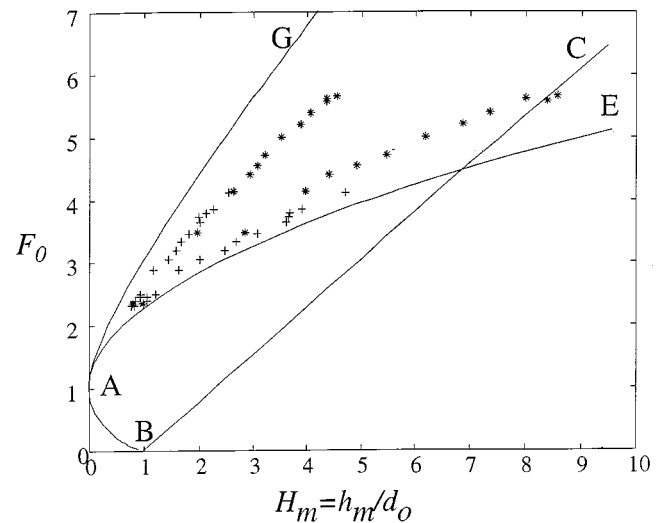

FIG. 9. Parameters of the runs when transitions were observed, compared with the theoretical curves identified in Fig. 1. Sluice gate heights are: + $d_0 = 0.0107$ m, * $d_0 = 0.0052$ m. The two lowest values with * have $d_0 = 0.0153$ m.

the hydraulic jump moves away from the location of the new stationary solution if it is displaced by an infinitesimal amount.

Some experimental observations using two different devices have demonstrated the existence of the multiple states, and provided support for the theory. Although the new flow solution could not be observed, the presence of multiple equilibria within the theoretically expected parameter range was confirmed, consistent with the observations of Lawrence,[4] with two different experimental configurations. Hysteresis was easily obtained in these two devices. They can be used for classroom demonstrations of the phenomenon. Visible waves on the water surface arose from geometric irregularities in the walls and floor, and the wave activity was very obvious when the flow was close to the AE transition in Figs. 1, 9. And with a smoother device, the transition from supercritical to subcritical flow at the crest may be moved even closer to AE than shown in Fig. 9.

The behavior observed here has some parallels with the more general phenomenon of forced nonlinear oscillators near resonance. Such systems may be characterized by a parameter (Γ, say, which for the present experiments could be identified with H) that measures the amplitude of the forcing, or of the nonlinearity, or a combination of both. A generic example is the forced Duffing equation.[9] Here, for small values of Γ there is a single solution for all values of the forcing frequency ω, but as Γ increases this solution curve folds over to give three solutions, of which the upper and lower are stable but the middle one is unstable. A second example occurs in weakly nonlinear two-layer baroclinic instability,[10] and a third example is the multiple equilibrium of thermohaline flows.[11–13] Experimental examples of multiple flow states are described by Whitehead et al.[14] The present system therefore constitutes a new member of the family that exhibits this form of behavior, in which the parameter corresponding to Γ is a combination of F_0 and H_m centered in the region GAE of Figs. 1 and 2.

The two devices described in Sec. IV were stationary flumes mounted on a solid base. Two additional small portable devices with the design of Fig. 7 have been constructed for educational demonstrations. Their channel lengths are 0.47 and 0.24 m, respectively, and their widths are 0.047 and 0.025 m, respectively. They easily reproduce the phenomena described for the laboratory apparatus when held steadily by hand. In addition, it is easy to manually balance the unstable hydraulic jump derived in Sec. II. We simply begin with the slope zero so that the flow is supercritical all along the channel. Then the slope is slowly increased ($\theta < 0$) until a hydraulic jump begins to form at the downstream end of the channel. As soon as the jump moves upstream, the angle is decreased until the jump stops. The angle is further decreased if the jump moves upstream again; or the angle is increased if the jump moves downstream again. The jump moves with typical speeds of 0.01 ms^{-1}, so the stabilizing adjustments are easy to make. If stabilizing adjustments cease, the jump invariably leaves the channel as predicted by the stability theory. A similar stabilization can be obtained in the larger of the two devices by altering the volume flux with a faucet or by pinching the hose that feeds the water into the device, but it is considerably more difficult. The experiment thereby shows that it is possible to stabilize an unstable branch of such a solution using the correct stabilizing feedback between either slope angle or volume flux and jump position. It is even conceivable that an appropriate elastic relationship between slope angle and weight in the channel would stabilize this jump completely, but such a relation has not yet been worked out.

[1] P. G. Baines, *Topographic Effects in Stratified Flows* (Cambridge University Press, Cambridge, 1995).

[2] L. J. Pratt, "A note on nonlinear flow over obstacles," Geophys. Astrophys. Fluid Dyn. **24**, 63 (1983).

[3] P. G. Baines and P. A. Davies, "Laboratory studies of topographic effects in rotating and/or stratified fluids," in *Orographic Effects in Planetary Flows* (GARP publication No. 23, WMO/ICSU, 233, 1980).

[4] G. A. Lawrence, "Steady flow over an obstacle," J. Hydraul. Eng. **113**, 981 (1987).

[5] K. Lofquist, "Flow and stress near an interface between stratified fluids," Phys. Fluids **3**, 158 (1960).

[6] A. D. D. Craik, R. C. Latham, M. J. Fawkes, and P. W. F. Gribbon, "The circular hydraulic jump," J. Fluid Mech. **112**, 347 (1981).

[7] X. Liu and J. H. Lienhard V, "The hydraulic jump in circular jet impingement and in other thin liquid films," Exp. Fluids **15**, 108 (1993).

[8] C. T. Avedisian and Z. Zhao, "The circular hydraulic jump in low gravity," Proc. R. Soc. London, Ser. A **456**, 2127 (2001).

[9] R. Grimshaw, *Nonlinear Ordinary Differential Equations* (Blackwell, Oxford, 1990).

[10] R. A. Plumb, "Forced waves in a baroclinic shear flow. Part 1: Undamped evolution near the baroclinic instability threshold," J. Atmos. Sci. **36**, 205 (1979).

[11] H. Stommel, "Thermohaline convection with two stable regimes of flow," Tellus **13**, 224 (1961).

[12] J. Marotzke, "Ocean models in climate problems," in *Ocean Processes in Climate Dynamics: Global and Mediterranean Examples*, edited by P. Malanotte-Rizzoli and A. R. Robinson (Kluwer, Dordrecht, 1994), p. 79.

[13] J. Whitehead, "Thermohaline ocean processes and models," Annu. Rev. Fluid Mech. **27**, 89 (1995).

[14] J. A. Whitehead, W. G. Lawson, and J. Salzig, "Multistate flow devices for geophysical fluid dynamics and climate," Am. J. Phys. **69**, 546 (2002).